International Journal of Heat and Mass Transfer 229 (2024) 125737

Contents lists available at ScienceDirect

International Journal of Heat and Mass Transfer

journal homepage: www.elsevier.com/locate/ijhmt

Multi-pulse thermoreflectance imaging with structure function analyses for measuring thermophysical properties of microscale heterostructures

Zhao-Yang Liu [1], Zhi-Ke Liu [1], Guang Yang, Bing-Yang Cao [*]

Key Laboratory for Thermal Science and Power Engineering of Ministry of Education, Department of Engineering Mechanics, Tsinghua University, Beijing, 100084, China

ARTICLE INFO

Keywords:
Thermoreflectance thermal imaging
Thermal structure function
Semiconductor heterostructure
Thermophysical property

ABSTRACT

The thermophysical properties of nano/microscale heterostructures play a crucial role in the performance and reliability of electronics. However, existing measurements encounter several challenges, including detecting multiple parameters synchronously and reliance on reference samples etc. In this study, we propose a multi-pulse thermoreflectance thermal imaging (TTI) combining with structure function algorithm, achieving simultaneous measurement of the thermal conductivities, specific heat capacities, and thermal boundary resistances (TBRs) of microscale heterostructures. A non-iterative methodology is established and the singular model parameter is evaluated through transient heat conduction modeling. We delineate criteria for thermal transient testing and achieve high-precision measurements over a broad time range by employing a multi-pulse strategy with a TTI system with a 50 ns temporal resolution. Our experimental measurements on a microscale Silicon-on-Insulator (SOI) sample validate the method's effectiveness. The measured thermophysical properties, including thermal conductivities of the device layer and handle wafer, TBR, and specific heat capacity of the device layer, exhibit a relative error of <10% compared to prior studies. Our approach presents an effective solution for precise thermal characterization within modern electronic devices.

1. Introduction

Heterostructures are the basic building blocks of nearly all kinds of semiconductor electronics [1], comprising layers of different solid materials, often involving combinations of metal-semiconductor interfaces, *p-n* junctions, semiconductor heterojunction interfaces, or metal-oxide-semiconductor structures, etc. The fabrication of heterostructures typically involves epitaxial growth techniques such as molecular beam epitaxy (MBE) [2] or chemical vapor deposition (CVD) [3]. Additional techniques, such as ion-implementation in Silicon-on-Insulator (SOI) [4], and fusion-bonding for Ga_2O_3/SiC composite wafers [5], are also employed. The precise control of deposition thickness and interface matching in heterostructures allows for the realization of advanced electronic devices with intricate designs [6,7]. With the escalating power density, working frequency, and integration density, heat dissipation has become a bottleneck in electronics devices, such as power electronics, radio frequency (RF), and microprocessors [8,9].

Characterizing the thermophysical properties of heterostructures is becoming more and more essential for addressing the thermal management challenges in electronics. In multilayer heterostructure, steady-state thermal behavior hinges on the thermal conductivities of films and substrates, as well as thermal boundary resistances (TBRs). Additionally, the specific heat capacities of films and substrates are also essential for transient characteristics. These multiple thermophysical properties serve as fundamental input parameters for device electro-thermal simulations and design, and eventually for their lifetime and reliability. So far, the database has not been completed yet as the technology node shrinks and new materials emerge continually. Moreover, in micro-and nanoscale realms, heat conduction is influenced by geometric dimensions [10,11], doping [12,13], strain [14], and defect [15], causing changes in macroscopic properties across different products.

Researchers have recently developed several experimental techniques for characterizing thermophysical properties in heterostructures. Ultrafast laser-based transient thermoreflectance (TTR) methods, such as time-domain thermoreflectance (TDTR) and frequency-domain thermoreflectance (FDTR), involve heating with a pump beam and detecting the reflectance changes with a probe beam to extract target properties [16,17]. While effective for nanoscale thin films, the shallow thermal penetration depth limits signal sensitivity to TBR and substrate for

* Corresponding author.
E-mail address: caoby@mail.tsinghua.edu.cn (B.-Y. Cao).
[1] These authors contributed equally.

https://doi.org/10.1016/j.ijheatmasstransfer.2024.125737
Received 22 February 2024; Received in revised form 15 May 2024; Accepted 17 May 2024

Nomenclature

a	Unit step response, K W^{-1}.
A_{eff}	Effective heat conduction area, m^2.
c_v	Specific heat capacity per volume, J m^{-3} K^{-1}.
C	Thermal capacitance, J K^{-1}.
d	Thickness of the film, m.
k	Thermal conductivity, W m^{-1} K^{-1}
M	Derivative of unit step response, $\equiv da/dz$.
N	Number of layers.
P	Heat flux(dissipation power), W.
q	Heat flux density, W m^{-2}.
r	Thermal boundary resistance, m^2 K W^{-1}.
R	Thermal resistance, K W^{-1}.
t	Time variable, s.
T	Temperature, K.
T_j	Junction temperature, K.
T_0	Initial temperature, K.
W	Weight function.
x,y	Cartesian coordinates.
z	Logarithmic time variable.

Greek symbols

γ	Reflectivity.
σ_{TR}	Thermoreflectance coefficient.
χ	Fitted slope of initial temperature response.
Ψ	Time-constant spectrum.
ΔT_j	Temperature change of junction, $\equiv T_j - T_0$, K.
ΣC	Cumulative thermal capacitance, J K^{-1}.
ΣR	Cumulative thermal resistance, K W^{-1}.

Subscripts

f	Film.
I	Interface.
sub	Substrate.
i	Index of the film layer.

Superscripts

(n)	Iterations.

micrometer-scale film heterostructures [18]. In steady-state thermoreflectance (SSTR), reducing the laser frequency to the order of 100 Hz enhances sensitivity to TBR, but a bare substrate reference sample remains necessary in practice [5,19]. Scanning thermal microscopy (SThM) uses a thermally sensitive probe placed on an atomic force microscopy (AFM) head to measure in-plane temperature maps (spatial resolution ~1 nm) and derive local thermophysical properties [20]. When applied to heterostructures, it requires reference bulk materials with known thermal conductivities for calibration and involves fitting from correlation, exhibiting poor sensitivity to the substrate [21]. Raman spectroscopy provides information on nanoscale thermal transport through Raman scattering [22]. However, its temperature uncertainty (~5 K) and spatial resolution (~1 μm) limit its application in measuring thermophysical properties [23,24]. In comparison to point-by-point temperature measurement methods, full-field measurement approaches, such as infrared thermography (IR) and thermoreflectance thermal imaging (TTI), have shown potential in assessing thermophysical properties. Leveraging the high spatial resolution of TTI, researchers have measured micro-and nanoscale single-layer films [25]. Liu et al. proposed a pulsed thermoreflectance imaging (PTI) method for heterostructure by analyzing spatiotemporal measurements with iterative FEM fitting [26].

Turning now to electrical methods, the differential 3ω method excels in measuring the thermal conductivity of thin films [27]. The thermal response to applied 1ω AC heating is measured with the 3ω voltage oscillation on the sensor and analyzed based on a series of samples with varying film thickness. As the fitting intercept contains contributions of the sensor-film TBR, the film-substrate TBR, and the substrate thermal conductivity, characterizing the TBR and substrate of a sample proves challenging [28]. The two-sensor 3ω-2ω method [28] and three-sensor 3ω-2ω method [29] are proposed to simultaneously measure the film, TBR, and substrate within an individual heterostructure. However, careful sensor layout design is required in sample preparation, and FEM fitting is needed in the analysis procedure.

It can be summarized that existing measurement methods for heterostructures face three primary limitations as follows. Firstly, achieving synchronous sensitivity to films, interfaces, and substrate proves challenging. For instance, TTR demonstrates good measurability of nanofilms but struggles to detect the substrate simultaneously. Secondly, reference samples are necessary for calibration or analysis, reflecting the difficulty in decoupling and solving multi-parameter inverse problems. Thirdly, iterative FEM fitting is consistently relied upon for analyzing target properties, leading to increased time and computational costs. These indicate the necessity to develop an efficient approach for measuring the thermophysical properties in typical semiconductor heterostructures.

In the field of electronics package testing, the structure function method stands out as a rapid and non-destructive thermal characterization approach. Initially proposed by Szekely, it evaluates the thermal transient step response of device packages based on thermoelectric analogy [30,31]. The core method, i.e., the structure function algorithm, includes deconvolution and network conversion. While the structure function method has demonstrated its versatility through applications in LED [32], IGBT [33], GaN HEMTs [34], and other semiconductor devices, these studies primarily focused on extracting macroscopic heat conduction information, such as junction-to-case thermal resistance and thermal contact resistance. Extracting the thermal conductivity of a single plate from the structure function has been achieved [35], but for heterostructures, the coexistence of multiple thermophysical properties introduces measurement complexity. Li et al. [36] measured the TBR of GaN-on-SiC via the structure function method but failed to provide the thermophysical properties of the thin film and the substrate. Up to this point, a measurement method utilizing the advantage of the structure function algorithm remains unestablished. Furthermore, existing experimental setups lack the requisite temporal resolution for measuring microscale structures. The temperature-sensitive electrical parameter (TSEP) method, as applied in the JEDEC JESD51-14 standard [37] for capturing the cooling response, is hindered by electrical effects when the heating current is switched off. Although researchers have managed to shorten the switching time from 100 μs to 1 μs [38], the temporal resolution remains insufficient for microscale films and interfaces near the junction.

In this work, we present an approach for the simultaneous measurements of multiple thermophysical properties within microscale heterostructures. While sustaining multi-parameter sensitivity through high temporal resolution testing, this method also extends the applicability of the structure function algorithm to eliminate the necessity for reference samples and FEM fitting. The measurement principles were first established to derive the measurement formulas for the thermal conductivities and specific heat capacities of the films and substrate, as well as the TBRs of interfaces. Subsequently, we detailed the determination of model parameters and the requirements for thermal transient testing, with a particular strategy proposed. Finally, experiments and analyses were conducted on a SOI sample to validate the effectiveness of

the proposed method, and the results were meticulously compared with prior studies.

2. Methods

2.1. Measurement principles

The comprehensive measurement scheme is illustrated in Fig. 1. To characterize a multilayer heterostructure, consisting of N layers of thin films on a substrate, along with a total of N interfaces between adjacent layers, a series of experiments and analyses are conducted.

Upon preparing the sample, a sudden heating step is uniformly applied to the surface of the heterostructure under test, and the thermal step response is measured using either electrical or optical methods over a specific time series. To further analyze the measured thermal step response, the structure function algorithm [30,31] is implemented. The input data constitutes the unit step response:

$$a(t) = \frac{T_j(t) - T_0}{P} \tag{1}$$

where $T_j(t)$ is the transient junction temperature, T_0 is the initial temperature, P is the heat flux (or dissipation power). Then a convolution-type equation is derived:

$$\frac{\mathrm{d}a(z)}{\mathrm{d}z} = \Psi(z) \otimes W(z) \tag{2}$$

where $z = \ln t$ is logarithmic time variable, $\Psi(z)$ is the time-constant spectrum, and $W(z)$ is the weight function given as:

$$W(z) = \exp(z - \exp(z)) \tag{3}$$

Consequently, the time-constant spectrum $\Psi(z)$ is calculated by deconvoluting the first derivative of the unit step response with respect to the logarithmic time variable. Among various deconvolution algorithms, Bayesian deconvolution shows superior spectral resolution [39] (also see Supplementary material):

$$\Psi_m^{(n+1)} = \Psi_m^{(n)} \Sigma_q \frac{W_{qm} M_q}{\Sigma_p M_{qm} \Psi_p^{(n)}} \tag{4}$$

where M_q, W_q are discrete form of $\mathrm{d}a/\mathrm{d}z$ and $W(z)$, $\Psi_m^{(n)}$ is the result of the nth iteration. Once the time-constant spectrum with high resolution is obtained, a Foster-form network is constructed using uniform discretization and Simpson integration. As the Foster-form network lacks physical meaning, it is crucial to convert it into an equivalent Cauer-form network [40], with the equivalent representation being the cumulative structure function.

Following the derivation of the cumulative structure function, each layer within the heterostructure can be distinctly identified. Adhering to heat conduction theory, the films and substrate exhibit relatively higher thermal conductivity and greater geometric thickness compared to the interfaces. This characteristic is reflected in the structure function, where these layers manifest as linear segments or slopes. Conversely, the interfaces feature higher thermal resistance and lower thermal capacitance, presenting as platforms in the structure function. The intrinsic characteristics of the structure function enable the identification of the boundary between the "slope" and the "platform". This distinction allows for the separation of cumulative thermal resistance $R_{f1}, R_{f2}, \cdots, R_{fN}$ of films, cumulative thermal capacitance $C_{f1}, C_{f2}, \cdots, C_{fN}$ of films, and cumulative thermal resistance $R_{I1}, R_{I2}, \cdots, R_{IN}$ of interfaces. For the identification of the substrate, differential structure function K_{sub} is fitted based on the linear segment of the substrate. This analysis approach effectively eliminates the artifact at the end of structure function introduced by non-isothermal boundary or incomplete response (S2, Supplementary Material).

Finally, the measurement formulas of the target thermophysical properties are given as follows ($i = 1, 2, \ldots, N$):

$$k_{fi} = \frac{d_{fi}}{R_{fi} A_{eff}} \tag{5}$$

$$c_{v,fi} = \frac{C_{fi}}{d_{fi} A_{eff}} \tag{6}$$

$$r_{i/i+1} = R_{Ii} A_{eff} \tag{7}$$

$$k_{sub} = \frac{K_{sub}}{c_{v,sub} A_{eff}^2} \tag{8}$$

where $k_{fi}, c_{v,fi}$ is the thermal conductivity and specific heat capacity per volume of the ith film, $r_{i/i+1}$ is the TBR of the ith interface, $k_{sub}, c_{v,sub}$ is the thermal conductivity and specific heat capacity per volume of the substrate. The thickness of the ith film d_{fi} is measured by optical methods, such as scanning electron microscope (SEM) [41] and white light interferometry [42]. The singular model parameter, namely the effective heat conduction area A_{eff}, is defined to correspond with the one-port equivalent Cauer network and will be expounded upon in Section 2.2 for thorough exposition.

2.2. Evaluation of effective heat conduction area

To apply the proposed measurement principles in practical testing, a detailed examination of the heat conduction within thermal transient testing is imperative. Under the condition of uniform heating across the sample surface, the effective heat conduction area corresponds to the sample's surface area. However, in the majority of heat transfer

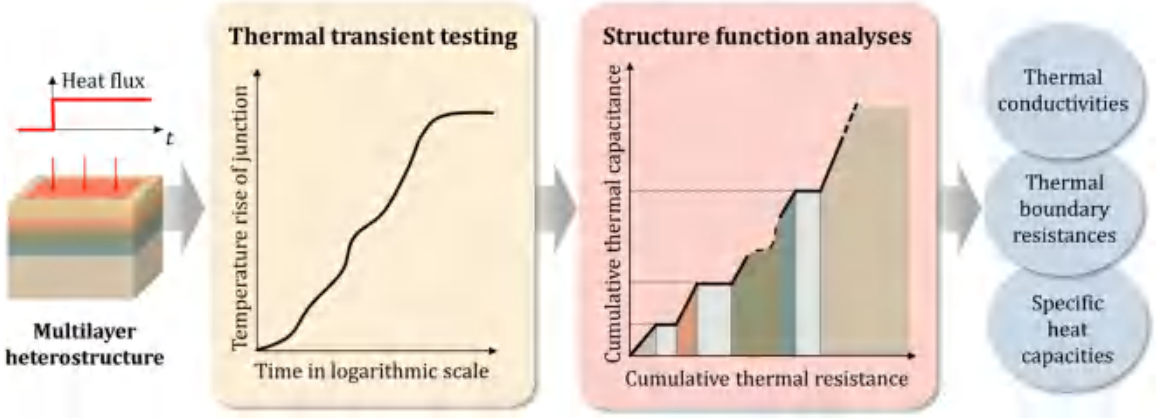

Fig. 1. Scheme for measuring thermophysical properties of a microscale multi-layer heterostructure.

experiments where the heat source occupies only a fraction of the surface area, it becomes essential to estimate the effective heat conduction area.

As illustrated in Fig. 2(a), when the area of the heat source on the upper surface significantly exceeds the total thickness of the sample, heat predominantly conducts in a one-dimensional manner along the thickness direction to correspond with a one-port equivalent Cauer network, referred to as "quasi-1D". As shown in Fig. 2(b), its initial temperature response can be modeled as transient 1D conduction in a semi-infinite plate under a constant heat flux boundary condition [43], with a spatiotemporal temperature field described by:

$$T(x,t) - T_0 = 2q\sqrt{\frac{t}{\pi k c_v}}e^{-\eta^2} - \frac{qx}{k}erfc(\eta) \tag{9}$$

where $\eta = \frac{x}{\sqrt{4at}}$ is a dimensionless quantity, $\mathrm{erfc}(\eta) = 1 - \frac{2}{\sqrt{\pi}}\int_0^{\eta} e^{-\eta^2}d\eta$ is complementary Gaussian error function, q is the heat flux density. Therefore, the transient response of junction temperature is expressed as:

$$T_j(t) = T(x=0,t) = T_0 + \frac{2q}{\sqrt{\pi k c_v}}\sqrt{t} \tag{10}$$

Then the effective heat conduction area is evaluated by fitting the initial response:

$$A_{\mathrm{eff}} = \frac{2P}{\chi\sqrt{\pi k_0 c_{v0}}} \tag{11}$$

where χ is the fitted slope of $T_j(\sqrt{t}\ )$ in the range of $t_s - t_{\mathrm{cut}}$, P is the heat flux, k_0, c_{v0} is the thermal conductivity and the specific heat capacity near junction. In practice, a thin film with known properties can be deposited on the top of the heterostructure for both parameter determination and electrical insulation.

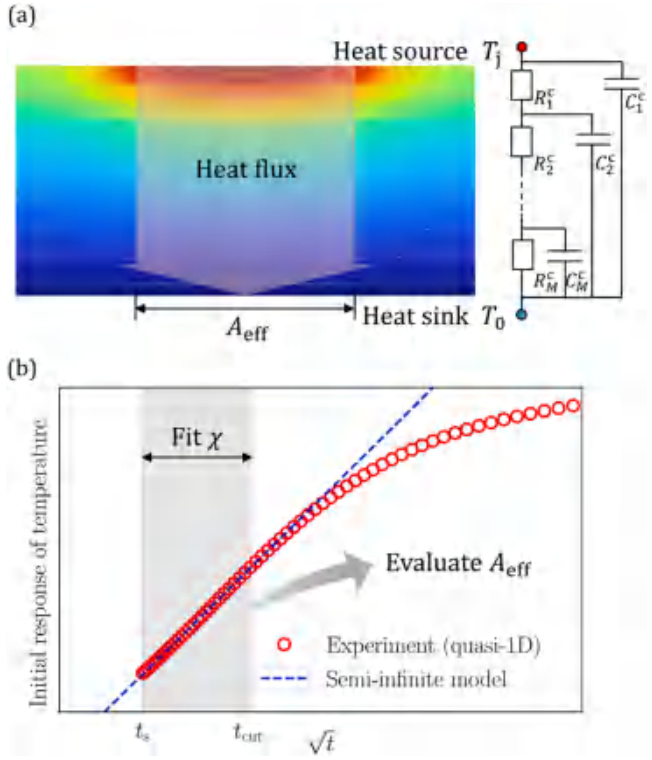

Fig. 2. Model parameter determination. (a) Quasi-1D heat conduction model and equivalent Cauer network. (b) Evaluation of effective heat conduction area by fitting the initial temperature response.

2.3. Criteria for thermal transient testing

Moreover, the experimental setup must fulfill specific criteria for the characterization of the target thermophysical properties. Firstly, the temperature measurement system should feature both sufficiently high temporal resolution and temperature resolution. Secondly, the heating step is required to mimic an ideal step function, ensuring a minimal rise time for voltage/heating power, which is essential for the derivation of the correct structure function (See Supplementary material).

For a particular application, thermoreflectance thermal imaging (TTI) was employed to measure the junction temperature of heterostructure samples during testing. The fundamental testing principle hinges on the linear relationship between the reflectivity change $\Delta\gamma$ and the temperature change ΔT within a temperature range of a few degrees [26,44,45]

$$\frac{\Delta\gamma}{\gamma} = \left(\frac{1}{\gamma}\frac{\partial\gamma}{\partial T}\right)\Delta T = \sigma_{\mathrm{TR}}\Delta T \tag{12}$$

where σ_{TR} is the thermoreflectance coefficient.

The testing system, illustrated in Fig. 3(a), involves illuminating the surface of the sample with an LED (530 nm, collimated) and collecting the reflected signal with a detector (acA2040-90umNIR, equipped with an ams CMV4000 sensor). The minimal pulse width of the probe LED is 50 ns for high temporal resolution. The temperature change maps were derived from the recorded reflectivity maps using Eq. (12). Each data point is averaged from multiple frames, achieving a temperature uncertainty <0.5 K. In order to attain an approximately ideal step response in the experiment, a signal generator with a rising edge of 20 ns-100 ns, such as the Ultra-Fast Pulse Measure Unit (Keithley 4225-PMU), was

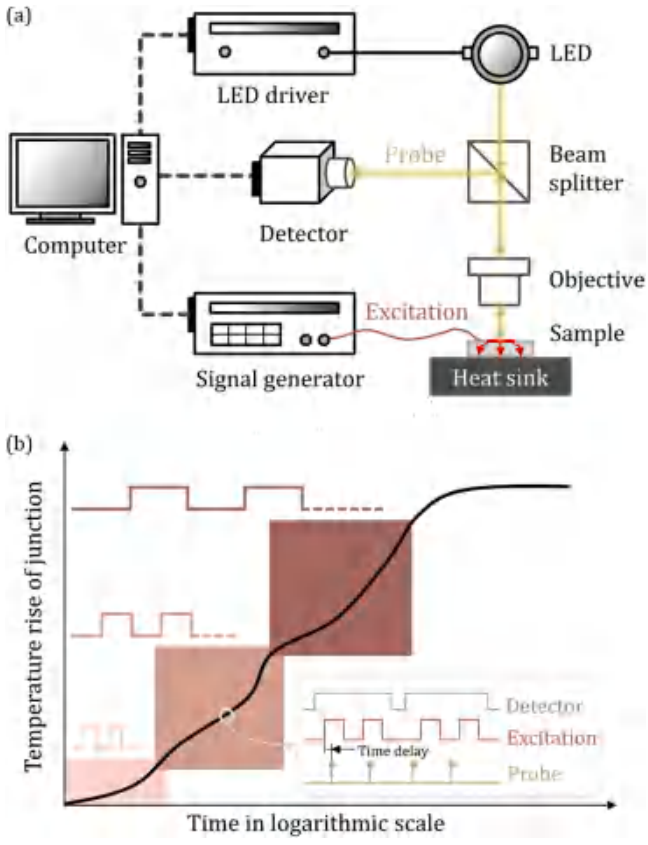

Fig. 3. Schematic of TTI transient thermal testing. (a) System setup. (b) A multi-pulse heating strategy. The tunable time delay of the probe pulses relative to the excitation dictates the sampling time of the thermal step response. Different groups of excitations were applied for high-resolution measurement over a broad time range.

chosen.

Furthermore, a multi-pulse heating strategy was devised to enable accurate measurements over a broad time range (Fig. 3(b)). Due to the proportional relationship between the probe LED pulse width and the detector exposure time, the accuracy of the initial segment of temperature measurement diminishes with prolonged heating time. Therefore, a hybrid approach was adopted: the initial segment of the step response was measured using short heating pulses, and the latter segment was measured using long heating pulses. Multiple sets of test data were then concatenated to achieve a high-time resolution transient thermal response across a time range spanning from tens of nanoseconds to hundreds of milliseconds.

It should be noted that any testing system and strategy that meets the above two criteria can be employed to acquire the thermal step response for extracting thermophysical properties.

3. Results and discussion

Tests and analyses were conducted on a representative Silicon-on-insulator (SOI) heterostructure to evaluate the viability and precision of the proposed method. As shown in Fig. 4(a), the SOI wafer under test comprises a P-type silicon device layer (~ 50 μm), a P-type silicon handle wafer (~400 μm), and a SiO_2 buried oxide (~2 μm) sandwiched in between. An insulation layer (~2 μm) was deposited with plasma-enhanced chemical vapor deposition (PECVD) on the device layer to prevent leakage during operation. Eventually, an Au heater was fabricated with electron beam lithography (EBL), metallization, and lift-off. Fig. 4(b) presents a top-down view of the pads and the snake-like heater, strategically designed for the quasi-1D heat conduction throughout the experiment (comparison of different designs can be found in S7, Supplementary Material).

Following the sample preparation, the transient temperature rise of the heater was measured through transient TTI experiments (Fig. 5). Prior to the formal testing, we first calibrated the thermoreflectance coefficient of the Au heater under 530 nm illumination, yielding a uniformly distributed value of -3.12×10^{-4} K^{-1}. The thermal step response was then measured using the multi-pulse heating strategy detailed in Section 2.3. The temperature distribution of the snake-like heater was effectively mapped over a wide time range from 50 ns to 30 ms, which was deemed sufficient for heat propagation from the top film to the bottom substrate.

Consequently, the junction temperature was defined as the average temperature rise of the heater:

$$\Delta T_j(t) = \Delta\,\overline{T}_{heater} = \frac{\int_{heater}(T(x,y;t) - T_0)\mathrm{d}x\mathrm{d}y}{\int_{heater}\mathrm{d}x\mathrm{d}y} \tag{13}$$

After obtaining the junction thermal step response, the analysis procedure outlined in Section 2.1 and Section 2.2 was executed to derive multiple thermophysical properties within the SOI heterostructure. Accuracy of the algorithm was pre-validated through case studies (S6, Supplementary Material), utilizing a double-precision program running single core on a system equipped with an i9 12900K CPU. The first step in this process was to calculate the effective heat conduction area by fitting the initial response (Fig. 6(a); details of pretreatment can be found in Supplementary material). Subsequently, the structure function algorithm was employed: the derivative of the thermal step response served as the initial value for Bayesian deconvolution, facilitating the derivation of the time-constant spectrum (Fig. 6(b)). It's worth noting that the LOWESS algorithm was utilized to smooth the sampling response before numerical differentiation [46]. Given the substantial thickness variations among the layers of the heterostructure, characteristic peaks emerged over a broad time range in the spectrum. The number of these peaks include not only the thermal characteristics of the sample but also artifacts of data noise and numerical deconvolution. Finally, a cumulative structure function was obtained through a judicious combination of iterations and network order (Fig. 6(c)). As heat generated from the heater and sequentially propagated from top to bottom (insulation layer →device layer →buried oxide →handle wafer), the structure function had a shape of "platform →slope →platform →slope" correspondingly. The device layer and the handle wafer correspond to the two "slopes" respectively due to the high thermal conductivity of silicon. In comparison to silicon, the insulation layer and buried oxide exhibited considerably lower thermal conductivities, resulting in the appearance of two distinct "platforms" in the corresponding segments of the structure function. This delineation allowed

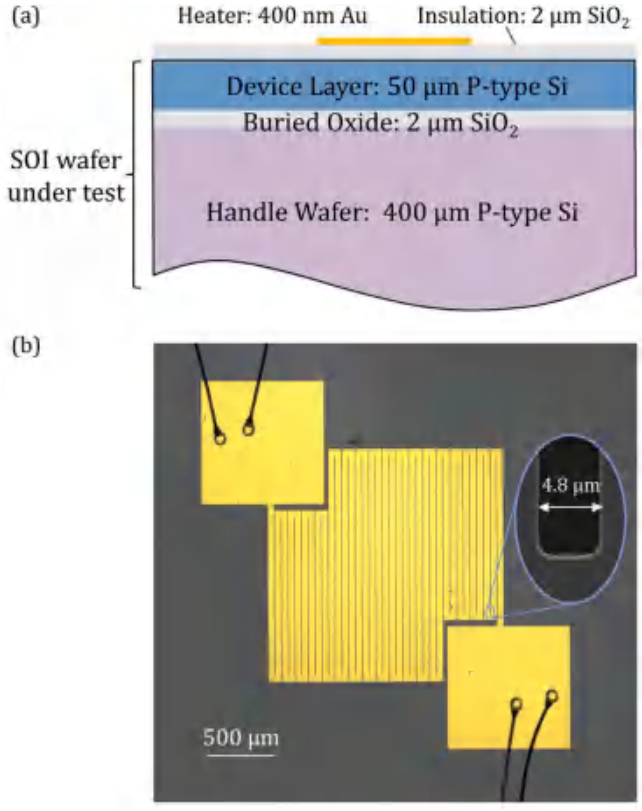

Fig. 4. SOI sample under test. (a) Longitudinal structure. (b) The top view is taken under the microscope; the inset image shows the details of the heater as observed by scanning electron microscopy.

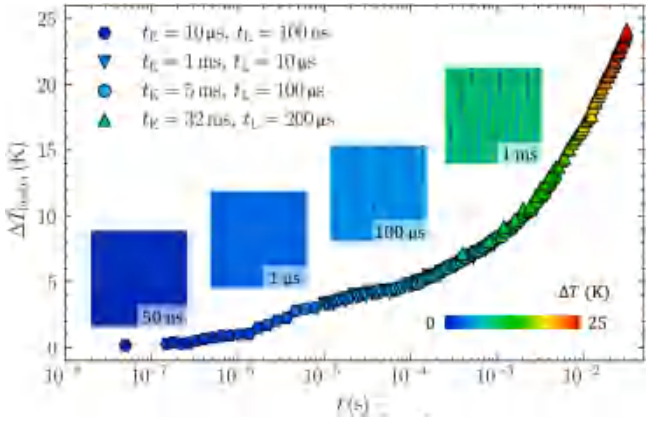

Fig. 5. Transient temperature rise of the heater measured with TTI. (t_E: pulse width of square-wave excitation, t_L: LED pulse width) The inset images are temperature maps at typical time points. According to the multi-pulse heating strategy, four different combinations of excitation pulses and probe pulses are applied to accurately measure the long time-span step response from 50 ns to 30 ms. The Joule heating power was measured to be 4.13 W.

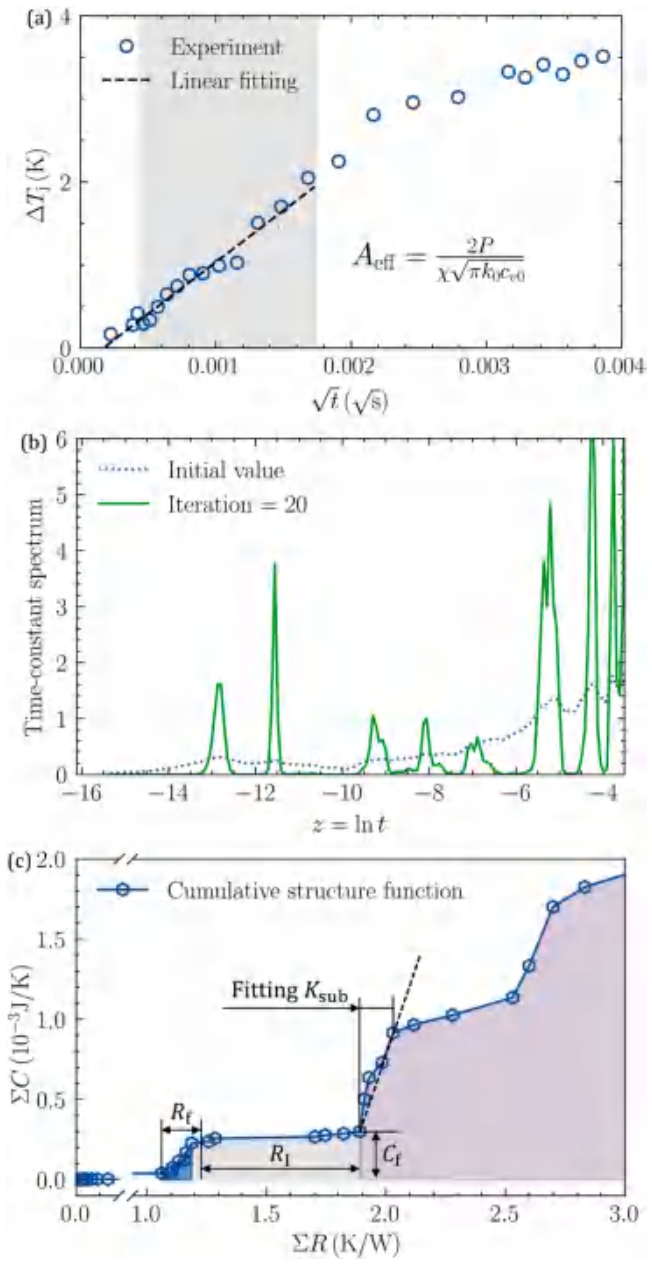

Fig. 6. Analysis of the measured thermal step response. (a) Fitting the initial response between 200 ns and 3 μs to calculate A_{eff} = 3.14 mm^2. (b) Time-constant spectrum by Bayesian deconvolution with the initial value of dα /dz after pretreatment. (c) Cumulative structure function. The thermal resistance R_f and thermal capacitance C_f of film, thermal resistance R_I of the interface, and differential structure function K_{sub} of handle wafer can be identified.

for the determination of the thermal resistance R_f and thermal capacitance C_f of film, thermal resistance R_I of Si/Si interface, and differential structure function K_{sub} of handle wafer.

Finally, the thermophysical properties in the SOI wafer were deduced from Eqs. (5)-(8):

$$k_f = \frac{d_f}{R_f A_{\text{eff}}} \tag{14}$$

$$c_{v,f} = \frac{C_f}{d_f A_{\text{eff}}} \tag{15}$$

$$r_{Si/Si} = R_I A_{\text{eff}} \tag{16}$$

$$k_{\text{sub}} = \frac{K_{\text{sub}}}{c_{v,\text{sub}} A_{\text{eff}}^2} \tag{17}$$

Table 1 presents the measured thermophysical properties at 300 K, accompanied by theoretical values for comparison. The measured thermal conductivities were found to be 109.2 ± 14.1 W m^{-1} K^{-1} for the device layer and 139.5 ± 22.9 W m^{-1} K^{-1} for the handle wafer. Considering the lower thermal conductivities of doped silicon layers compared to bulk intrinsic silicon due to phonon-impurity scattering, predictions for these layers fell within the range of 106–111 W m^{-1} K^{-1} and 130 W m^{-1} K^{-1}, respectively, with estimated doping concentrations of 1.6 × 10^{18}–4.4 × 10^{18} and 6.3 × 10^{14}–1.2 × 10^{16} [12,47,48]. Moving to the thermal boundary resistance between the silicon device layer and the handle wafer, the measured result was 2.099 ± 0.206 m^2 K MW^{-1}. In comparison, the equivalent interface thermal resistance was estimated to be in the range of 1.91–1.98 m^2 K MW^{-1} based on the experimental results reported by He et al. [49]. The measured value, slightly larger than the theoretical expectation, could be attributed to the existence of two Si/SiO$_2$ interfaces. In addition to the steady-state heat conduction characteristic, the specific heat capacitance of the device layer was extracted as 1.656 ± 0.141 J cm^{-3} K^{-1}, showing good agreement with the standard value in the database [50].

To conclude, our measurements successfully identified the multiple thermophysical properties within the SOI heterostructure. No reference samples of SOI were used in the experiments and only one response curve was measured in thermal transient testing. As the thermophysical properties of SOI were expressed as explicit functions in Eqs. (14)–(17), a non-iterative analysis approach was achieved without reliance on FEM fitting. According to the error propagation theory, the uncertainties of each parameter are all within 15% (refer to Supplementary material).

Furthermore, the applicability of this method extends to other cases through simulation, including a series of GaN-on-SiC heterostructures (as detailed in Supplementary material). Nevertheless, the quality of the measured transient response data and the pre-treatment methodology significantly impact the method's feasibility. Designing appropriate filters, such as LOWESS utilized in this study, becomes crucial for enhancing signal fidelity. The control experiment in SOI by simulation further supports this idea by mitigating the impact of data quality (as detailed in the Supplementary material). In addition, the quasi-1D hypothesis introduced some level of system error into our results. This prompts consideration for heat source designs that approach a uniform heat flux boundary, which may yield more favorable outcomes.

4. Conclusions

In this study, we have presented a novel method for simultaneously measuring multiple thermophysical properties, including thermal conductivities, thermal boundary resistances (TBRs), and specific heat capacities in microscale multilayer heterostructures. Our approach involves a systematic process, starting with the measurement of the thermal step response through high temporal resolution testing and proceeding to the analysis procedure based on the structure function algorithm. The derived cumulative structure function provides an

Table 1
Measured thermophysical properties of the SOI sample compared with previous studies (300 K). (k_f: thermal conductivity of the device layer, $c_{v,f}$: specific heat capacity per volume of the device layer, $r_{Si/Si}$: TBR between the device layer and the handle wafer, k_{sub}: thermal conductivity of the handle wafer).

	k_f [W m^{-1} K^{-1}]	k_{sub} [W m^{-1} K^{-1}]	$r_{Si/Si}$ [m^2 K MW^{-1}]	$c_{v,f}$ [10^6 J m^{-3} K^{-1}]
This work	109.2 ± 14.1	139.5 ± 22.9	2.099 ± 0.206	1.656 ± 0.141
Prior studies	106–111 [12]	130 [12,47]	1.91–1.98 [49]	1.63 [50]

equivalent representation of heat conduction characteristics within heterostructures. Finally, a non-iterative measurement is directly achieved based on the linear relationship between the target thermophysical properties and the cumulative thermal resistances/capacitances. To further apply these principles, we evaluate the singular model parameter, i.e., the effective heat conduction area, by quasi-1D heat conduction modeling. Additionally, we define criteria for the experimental system, implementing a practical approach that includes a thermoreflectance thermal imaging (TTI) system featuring a 50 ns temporal resolution and a multi-pulse heating strategy to achieve high-precision measurements over a broad time range.

For experimental validation, tests were conducted on a typical Silicon-on-Insulator (SOI) sample, featuring a snake-like heater on the device layer. The sample under test was excited and imaged over a wide time range from 50 ns to 30 ms in the transient TTI experiments. The proposed analysis procedure based on the structure function algorithm was executed to derive target thermophysical properties at 300 K. The measured thermal conductivities of the device layer and handle wafer, TBR of the interface, and specific heat capacities showed consistent agreement with previous studies, maintaining an uncertainty below 15%.

This study can facilitate thermophysical properties measurement in microelectronics through the exploration of the structure function method. Notably, our proposed method, demonstrating synchronous sensitivities to discrete components of heterostructures, obviates the need for reference samples in experiments and eliminates the reliance on FEM fitting during the analysis process. By effectively decoupling multiple parameters, our non-iterative testing scheme enables precise and efficient thermal characterization for complex semiconductor structures.

CRediT authorship contribution statement

Zhao-Yang Liu: Writing – original draft, Visualization, Software, Methodology, Investigation, Formal analysis, Conceptualization. **Zhi-Ke Liu:** Writing – review & editing, Methodology, Investigation. **Guang Yang:** Writing – review & editing, Methodology, Conceptualization. **Bing-Yang Cao:** Writing – review & editing, Supervision, Resources, Project administration, Funding acquisition, Conceptualization.

Declaration of competing interest

The authors declare that they have no known competing financial interests or personal relationships that could have appeared to influence the work reported in this paper.

Data availability

Data will be made available on request.

Acknowledgments

This study was financially supported by the National Natural Science Foundation of China (Nos. 52327809, 52425601, U20A20301, 52250273, and 82361138571), National Key Research and Development Program of China (No. 2023YFB4404104), and Beijing Natural Science Foundation (No. L233022).

Supplementary materials

See the Supplementary material for comparison of different deconvolution implementations (S1); effect of non-isothermal boundary condition and incomplete response (S2); necessity of minimizing excitation rise time (S3); details of pretreatment on thermal step response (S4); error analysis of SOI experiments (S5); simulations in more material systems (S6); simulation experiments on SOI (S7). Supplementary material associated with this article can be found, in the online version, at doi:10.1016/j.ijheatmasstransfer.2024.125737.

References

[1] Simon M. Sze, M.-K. Lee, Semiconductor Devices Physics and Technology, 3rd ed., Wiley, New York, 2012.
[2] W.P. McCray, MBE deserves a place in the history books, Nat. Nanotechnol. 2 (2007) 259–261.
[3] N. binti Hamzan, C.Y. Bin Ng, R. Sadri, M.K. Lee, L.-J. Chang, M. Tripathi, A. Dalton, B.T. Goh, Controlled physical properties and growth mechanism of manganese silicide nanorods, J. Alloys Compd. 851 (2021) 156693.
[4] G.K. Celler, S. Cristoloveanu, Frontiers of silicon-on-insulator, J. Appl. Phys. 93 (2003) 4955–4978.
[5] Y. Song, D. Shoemaker, J.H. Leach, C. McGray, H.-L. Huang, A. Bhattacharyya, Y. Zhang, C.U. Gonzalez-Valle, T. Hess, S. Zhukovsky, K. Ferri, R.M. Lavelle, C. Perez, D.W. Snyder, J.-P. Maria, B. Ramos-Alvarado, X. Wang, S. Krishnamoorthy, J. Hwang, B.M. Foley, S. Choi, Ga2O3-on-SiC composite wafer for thermal management of ultrawide bandgap electronics, ACS. Appl. Mater. Interfaces 13 (2021) 40817–40829.
[6] A.K. Geim, I.V. Grigorieva, Van der Waals heterostructures, Nature 499 (2013) 419–425.
[7] S. Tian, T. Wu, S. Hu, D. Ma, L. Zhang, Boosting phonon transport across AlN/SiC interface by fast annealing amorphous layers, Appl. Phys. Lett. 124 (2024) 042202.
[8] D.-S. Tang, B.-Y. Cao, Phonon thermal transport and its tunability in GaN for near-junction thermal management of electronics: a review, Int. J. Heat. Mass Transf. 200 (2023) 123497.
[9] M. Tadjer, T. Anderson, Thermal Management of Gallium Nitride Electronics, Woodhead Publishing, 2022.
[10] Y.-C. Hua, B.-Y. Cao, Phonon ballistic-diffusive heat conduction in silicon nanofilms by Monte Carlo simulations, Int. J. Heat. Mass Transf. 78 (2014) 755–759.
[11] Y.-C. Hua, B.-Y. Cao, The effective thermal conductivity of ballistic–diffusive heat conduction in nanostructures with internal heat source, Int. J. Heat. Mass Transf. 92 (2016) 995–1003.
[12] M. Asheghi, K. Kurabayashi, R. Kasnavi, K.E. Goodson, Thermal conduction in doped single-crystal silicon films, J. Appl. Phys. 91 (2002) 5079–5088.
[13] A.D. McConnell, S. Uma, K.E. Goodson, Thermal conductivity of doped polysilicon layers, J. Microelectromech. Syst. 10 (2001) 360–369.
[14] D.-S. Tang, G.-Z. Qin, M. Hu, B.-Y. Cao, Thermal transport properties of GaN with biaxial strain and electron-phonon coupling, J. Appl. Phys. 127 (2020) 035102.
[15] Y. Lee, S. Lee, G.S. Hwang, Effects of vacancy defects on thermal conductivity in crystalline silicon: a nonequilibrium molecular dynamics study, Phys. Rev. B 83 (2011) 125202.
[16] P. Jiang, X. Qian, R. Yang, Tutorial: time-domain thermoreflectance (TDTR) for thermal property characterization of bulk and thin film materials, J. Appl. Phys. 124 (2018) 161103.
[17] A.J. Schmidt, R. Cheaito, M. Chiesa, A frequency-domain thermoreflectance method for the characterization of thermal properties, Rev. Sci. Instrum. 80 (2009) 094901.
[18] Z. Cheng, F. Mu, L. Yates, T. Suga, S. Graham, Interfacial thermal conductance across room-temperature-bonded GaN/diamond interfaces for GaN-on-diamond devices, ACS. Appl. Mater. Interfaces 12 (2020) 8376–8384.
[19] J.L. Braun, D.H. Olson, J.T. Gaskins, P.E. Hopkins, A steady-state thermoreflectance method to measure thermal conductivity, Rev. Sci. Instrum. 90 (2019) 024905.
[20] Y. Zhang, W. Zhu, F. Hui, M. Lanza, T. Borca-Tasciuc, M.Muñoz Rojo, A review on principles and applications of scanning thermal microscopy (SThM), Adv. Funct. Mater. 30 (2020) 1900892.
[21] S. Gomès, P. Newby, B. Canut, K. Termentzidis, O. Marty, L. Fréchette, P. Chantrenne, V. Aimez, J.-M. Bluet, V. Lysenko, Characterization of the thermal conductivity of insulating thin films by scanning thermal microscopy, Microelectronics J. 44 (2013) 1029–1034.
[22] S. Xu, A. Fan, H. Wang, X. Zhang, X. Wang, Raman-based nanoscale thermal transport characterization: a critical review, Int. J. Heat Mass Transf. 154 (2020) 119751.
[23] R.J.T. Simms, J.W. Pomeroy, M.J. Uren, T. Martin, M. Kuball, Channel temperature determination in high-power AlGaN/GaN HFETs using electrical methods and Raman spectroscopy, IEEE Trans. Electron. Devices 55 (2008) 478–482.
[24] M. Kuball, J.W. Pomeroy, A review of Raman thermography for electronic and opto-electronic device measurement with submicron spatial and nanosecond temporal resolution, IEEE Trans. Device Mater. Reliab. 16 (2016) 667–684.
[25] T. Zhu, D.H. Olson, P.E. Hopkins, M. Zebarjadi, Heat diffusion imaging: in-plane thermal conductivity measurement of thin films in a broad temperature range, Rev. Sci. Instrum. 91 (2020) 113701.
[26] Z.-K. Liu, G. Yang, B.-Y. Cao, Pulsed thermoreflectance imaging for thermophysical properties measurement of GaN epitaxial heterostructures, Rev. Sci. Instrum. 94 (2023) 094902.
[27] C. Dames, Measuring the thermal conductivity of thin films: 3 omega and related electrothermal methods, Ann. Rev. Heat Transfer 16 (2013) 7–49.
[28] Y.-C. Hua, B.-Y. Cao, A two-sensor 3ω-2ω method for thermal boundary resistance measurement, J. Appl. Phys. 129 (2021) 125107.

[29] G. Yang, B.-Y. Cao, Three-sensor 3ω-2ω method for the simultaneous measurement of thermal conductivity and thermal boundary resistance in film-on-substrate heterostructures, J. Appl. Phys. 133 (2023) 045104.
[30] V. Székely, T. Van Bien, Fine structure of heat flow path in semiconductor devices: a measurement and identification method, Solid. State Electron. 31 (1988) 1363–1368.
[31] V. Székely, A new evaluation method of thermal transient measurement results, Microelectronics J. 28 (1997) 277–292.
[32] H.-H. Kim, S.-H. Choi, S.-H. Shin, Y.-K. Lee, S.-M. Choi, S. Yi, Thermal transient characteristics of die attach in high power LED PKG, Microelectronics Reliab. 48 (2008) 445–454.
[33] E. Deng, Z. Zhao, P. Zhang, X. Luo, J. Li, Y. Huang, Study on the method to measure thermal contact resistance within press pack IGBTs, IEEE Trans. Power Electron. 34 (2019) 1509–1517.
[34] X. Meng, M. Zhang, K. Duan, X. Zheng, Y. Zhai, S. Feng, Y. Zhang, Research on transient temperature rise measurement method for semiconductor devices based on photothermal reflection, IEEE Trans. Instrum. Meas. 72 (2023) 1–9.
[35] V. Szekely, W. Rencz, S. Torok, S. Ress, Calculating effective board thermal parameters from transient measurements, IEEE Trans. Components Packag. Technol. 24 (2001) 605–610.
[36] X. Li, S. Feng, Z. Feng, S. Pan, Y. Lv, K. Bai, X. Lu, J. Qin, Y. Zhang, A thermal boundary resistance measurement method based on a designed chip with the heat source separated from the temperature sensor, Appl. Phys. Lett. 122 (2023) 073501.
[37] JEDEC, JESD51-14 Standard: Transient Dual Interface Test Method for the Measurement of the Thermal Resistance Junction-to-Case of Semiconductor Devices with Heat Flow Through a Single Path, 2010. www.jedec.org.
[38] X. Li, S. Feng, C. Liu, Y. Zhang, K. Bai, Y. Xiao, X. Zheng, X. He, S. Pan, G. Lin, L. Bai, A drain–source connection technique: thermal resistance measurement method for GaN HEMTs using TSEP at high voltage, IEEE Trans. Electron. Devices 67 (2020) 5454–5459.
[39] K.A. Pareek, C. Grosse, M. Sternberg, D. May, M.A. Ras, B. Wunderle, Effect of different deconvolution methods on structure function calculation, in: 2020 26th International Workshop on Thermal Investigations of ICs and Systems (THERMINIC), 2020, pp. 97–104.
[40] V. Székely, On the representation of infinite-length distributed RC one-ports, IEEE Trans. Circuits Syst. 38 (1991) 711–719.
[41] W. Zhou, R. Apkarian, Z.L. Wang, D. Joy, Fundamentals of scanning electron microscopy (SEM), in: W. Zhou, Z.L. Wang (Eds.), Scanning Microscopy for Nanotechnology: Techniques and Applications, Springer, New York, 2007, pp. 1–40.
[42] B. Maniscalco, P.M. Kaminski, J.M. Walls, Thin film thickness measurements using scanning white light interferometry, Thin Solid Films 550 (2014) 10–16.
[43] M.N. Â–zisik, M.N. Özışık, Heat Conduction, John Wiley & Sons, 1993, pp. 115–117.
[44] Z.-K. Liu, Y. Shen, H.-L. Li, B.-Y. Cao, Observation of ballistic-diffusive thermal transport in GaN transistors using thermoreflectance thermal imaging, Rare Metals 43 (2024) 389–394.
[45] S. Sandell, E. Chávez-Ángel, A. El Sachat, J. He, C.M. Sotomayor Torres, J. Maire, Thermoreflectance techniques and Raman thermometry for thermal property characterization of nanostructures, J. Appl. Phys. 128 (2020) 131101.
[46] J. Yang, S. Feng, D. Shi, C. Yang, Thermal time-constant spectrum extraction method in AlGaN/GaN HEMTs, J. Semiconductors 36 (2015) 084003.
[47] G.A. Slack, Thermal conductivity of pure and impure silicon, silicon carbide, and diamond, J. Appl. Phys. 35 (2004) 3460–3466.
[48] W.R. Thurber, R.L. Mattis, Y.M. Liu, J.J. Filliben, Resistivity-dopant density relationship for boron-doped silicon, J. Electrochem. Soc. 127 (1980) 2291.
[49] P. He, L. Liu, L. Tian, Z. Li, Measurement of thermal conductivity of buried oxides of silicon-on-insulator wafers fabricated by separation by implantation of oxygen technology, Appl. Phys. Lett. 81 (2002) 1896–1898.
[50] P. Flubacher, A.J. Leadbetter, J.A. Morrison, The heat capacity of pure silicon and germanium and properties of their vibrational frequency spectra, Philos. Mag.: J. Theor. Exp. Appl. Phys. 4 (1959) 273–294.